PROCEEDINGS OF SCIENCE

Soft and Hard Diffraction at 7 TeV observed with CMS

Marta Ruspa (on behalf of the CMS Collaboration)*
University of Eastern Piedmont, Novara (Italy) and INFN-Torino (Italy) E-mail:
ruspa@to.infn.it

Recent measurements are presented of soft and hard diffractive processes in pp collisions at $\sqrt{s} =$ 7 TeV at the LHC using the CMS detector. Results are presented of the single- and double-diffractive cross section and of the inclusive differential cross section for events with a forward rapidity gap. A study of event yields when no particles are produced between two leading jets is also reported.

XXIV International Workshop on Deep-Inelastic Scattering and Related Subjects
11-15 April, 2016
DESY Hamburg, Germany

*Speaker.

PoS(DIS2016)197

1. Introduction

Two generic kinds of processes lead to the production of most of the final states in proton-proton (pp) collisions at LHC energies. The main and dominant contribution is related to semi-hard (multi)parton scattering, where the exchanged momenta amount to a few GeV, and the scattered quarks and gluons fragment into hadrons. In the second place, diffractive scattering in more peripheral pp interactions, where one or both the protons survive the collision and/or are excited into a low-mass state, contribute to between 15 and 25% of the inelastic cross section. Both such contributions are modelled phenomenologically in the existing Monte Carlo (MC) event generators; the model predictions generally differ between pre-LHC center-of-mass energies ($\sqrt{s} = 1.96$ TeV maximum) and those (7-8-13 TeV) reached at the LHC. Experimental results from LHC run I have been relevant for tuning the models.

Diffractive processes are characterized by the presence of at least one large rapidity gap (LRG), a region in rapidity devoid of particles. LRGs originate by a color singlet exchange (CSE) carrying the vacuum quantum numbers, usually referred to as Pomeron (IP) exchange. Consequently, one or both the incoming protons emerge almost unscated, carrying most of the beam energy, or dissociate into a low mass system. Figure 1 shows schematically non-diffractive (ND), single-diffractive (SD), and double-diffractive (DD) processes in pp collisions. The systems X and Y represent the dissociated protons and can be analyzed inclusively (inclusive processes) or can be a specific object (exclusive diffraction). When a hard scale is absent such processes, therefore termed as soft due to their large cross section, are a tool to model the final state of minimum-bias events, and to simulate the underlying event and pileup events. When a hard scale is present (e.g. when X includes high-p_T jets, W or Z bosons,...) perturbative QCD (pQCD) becomes applicable and the dynamics can be formulated in terms of partons. Existing data are successfully described by calculation based on the DGLAP evolution equations [1].

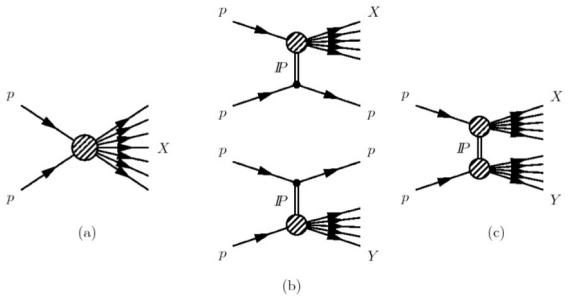

Figure 1: Schematic diagram of (a) non-diffractive, $pp \to X$, and diffractive processes with (b) single-dissociation, $pp \to pX$, and (c) double-dissociation $pp \to XY$.

Also consistent with diffractive processes are more specific rapidity gap topologies, e.g. the absence of particles between two leading jets (Fig. 2). Here, however, the absolute value of the four-momentum squared carried by the color-singlet exchange is much larger than in standard diffraction and such processes can be understood in the BFKL-inspired pQCD approach in terms of the exchange of a color-singlet gluon ladder, as first discussed in [2]. The study of jet-gap-jet events may allow to disentangle between BFKL and DGLAP dynamics.

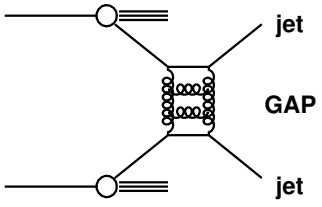

Figure 2: Schematic diagram of a dijet event with a rapidity gap between the jets.

This paper presents recent CMS measurements of soft (single and double diffractive cross sections and forward rapidity gap cross sections at $\sqrt{s}$ = 7 TeV) and hard (yields of events with rapidity gap between jets) diffraction. The CMS [3] detector is described elsewhere.

2. Inclusive diffractive cross section and rapidity gap cross section

Diffractive cross sections were measured [4] from a sample of 16.2 μb^{-1} integrated luminosity, collected by CMS at $\sqrt{s}$ = 7 TeV during the year 2010, when the LHC, still under commissioning, was running with a low average number of inelastic collisions per bunch crossing (pileup) of μ = 0.14, most suitable for LRG tagging. Online and offline, before the LRG requirement, a minimum-bias sample was selected corresponding to the total inelastic cross section, limited to using only the central CMS detector (-4.7 $\leq \eta \leq$ 4.7), where η is defined as $-ln[tan(\theta/2)]$, with θ the polar angle of the particle trajectory with respect to the anticlockwise-beam direction. The PYTHIA8-MBR (Minimum Bias Rockefeller) Monte Carlo [5] was used for the acceptance calculation, for the background subtraction and to extrapolate the measured cross sections to the low-mass region, to which the CMS detector is insensitive. The 4C tune [6] of the same generator was instead used as a systematic check.

Two experimental topologies, differing in the location of the gap, were used: forward pseudorapidity gap reconstructed at the edge of the detector on the negative η-side; central pseudorapidity gap reconstructed in the detector around $\eta \simeq 0$. The first topology is described by the variables η_{min}, defined as the lowest η of the particle candidates in the central detector. The central-gap topology is related to $\Delta\eta^0 = \eta^0_{max} - \eta^0_{min}$, with η^0_{max} (η^0_{min}) the closest-to-zero value of the pseudorapidity of the particle candidate on the positive (negative) η side of the detector. The distribution of η_{min} ($\Delta\eta^0$) is shown in Fig. 3 top (bottom) and compared to MC predictions. The data are dominated by ND events. Diffractive events appear as a flattening of the exponential fall off and populate the regions of high $\eta_{\rm min}$ and high $\Delta\eta^0$. Hence the cuts η_{min} > -1 and $\Delta\eta^0$> 3 were imposed. The CASTOR calorimeter (-6.6 $\leq \eta \leq$ -5.2) was used to tag the low-mass (3.2 GeV < M_x < 12 GeV) dissociated system in DD events, which, as shown by Fig. 3 top, amounts to half of the sample.

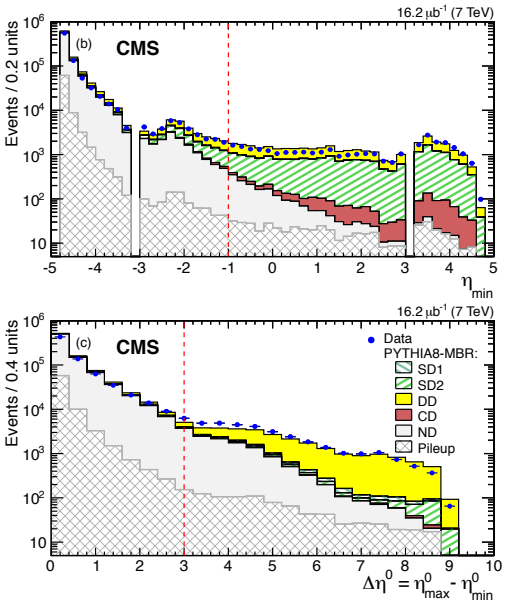

Figure 3: Detector level η_{min} (top) and $\Delta\eta^0$ (bottom) distributions for the minimum-bias sample compared to predictions of the PYTHIA8-MBR simulation, shown separately for the different processes and normalized to the luminosity of the data.

The SD and DD cross sections were extracted from the negative-side-gap sample. Their extrapolated values are shown in Fig. 4 left and right respectively as a function of the center-of-mass energy. and compared to the ALICE result [7] and to a compilation of lower center-of-mass energy measurements and theoretical models. The CMS data are consistent with a weak rise with energy of the SD and DD cross sections, as predicted by the models.

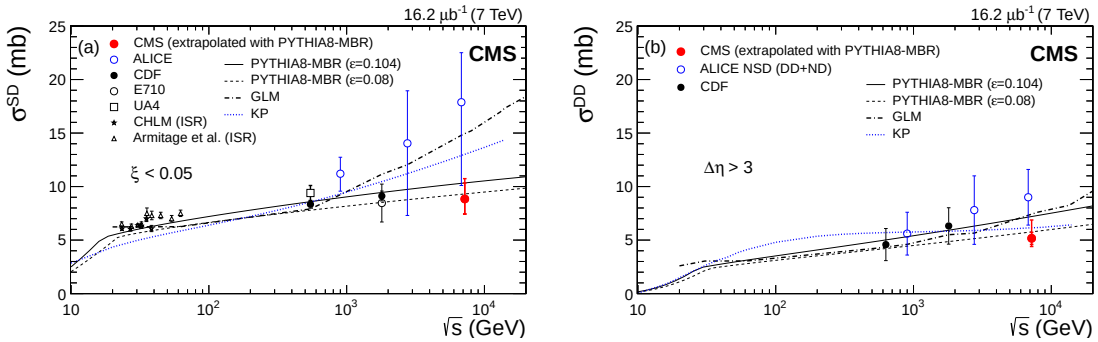

Figure 4: SD (left) and DD (right) cross sections as a function of $\sqrt{s}$. The CMS data are compared to the ALICE data [7], as well as to a compilation of measurements at lower $\sqrt{s}$ and of theoretical models (see [4] for references).

Given the impossibility to measure the whole mass of the diffractively dissociated system due to the limited forward coverage of the detector, alternatively one can measure the size of the corresponding pseudorapity gap. In each reconstructed event of the central-gap sample, the largest gap between each edge of the detector and the position in η of the first particle found in moving away from the edge is designated as the largest forward rapidity gap, $\Delta\eta^F$. The unfolded and fully corrected differential cross section of the forward gap size is shown and compared to a previous ATLAS measurement [8] in Fig. 5. The green band represents the total systematic uncertainty of the CMS measurement (included in the error bands in ATLAS case). It must be added that the hadron level definition is not exactly the same as CMS gap starts at $|\eta| \pm 4.7$, whereas ATLAS cross section is given for $|\eta| < 4.9$. The CMS result extends the ATLAS measurement by 0.4 unit of gap size.

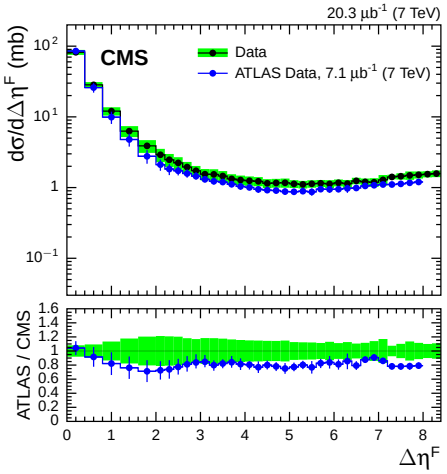

Figure 5: Differential cross section of the forward rapidity gap size, $d\sigma/d\Delta\eta^F$, compared to the ATLAS measurement described in the text.

3. Events with rapidity gap between jets

The data used for the measurement of event yields in the jet-gap-jet topology (Fig. 2) correspond to 8 pb^{-1} of integrated luminosity and were taken with the CMS detector in the year 2010 at $\sqrt{s}$ = 7 TeV with low pileup. Three non-overlapping samples of dijet events were used with different intervals of the transverse momentum of the second leading jet, p_T^{jet2}: 40-60 GeV, 60-100

GeV, and 100-200 GeV. The discrimination between CSE and non-CSE events was based on the charged multiplicity distribution, defined as the number of reconstructed tracks with $p_T \geq 0.2$ GeV in the fixed pseudorapidity interval $|\eta| < 1$. It is shown for the highest p_T interval in Fig. 6 (left), where the PYTHIA6 [9] simulation provides a good description of the data, with the exception of the lowest multiplicity bins, in which an excess of events is seen. The latter is well modelled by the HERWIG6 generator [10], which implements hard CSE according to the model by Mueller and Tang [2]. HERWIG was reweighted to describe the jet p_T spectrum. The simulation of MPI, not included in HERWIG, was provided by the JIMMY package [11].

The signal was defined as the ratio between the number of events with gap divided by the total number of dijet events. The former corresponds to the events exceeding the QCD (PYTHIA) background at low multiplicities. The shape of the multiplicity distribution for background events was estimated by a fit based on a negative binomial distribution (NBD) function. The fit was extrapolated to the lowest multiplicity bins and used to count and subtract the background. The non-CSE background constitutes about 10-15% of the events in the 0^{th} bin of the multiplicity distribution, about 25-30% in the first two multiplicity bins, and about 40-60% when the signal is integrated over the first three multiplicity bins. A second data-driven approach was used as a systematic check. Figure 6 right shows the track multiplicity distribution in the highest p_T^{jet2} bin after subtracting the background. A clear excess in the lowest p_T bins is observed over a flat continuum, in agreement with the predictions of HERWIG6.

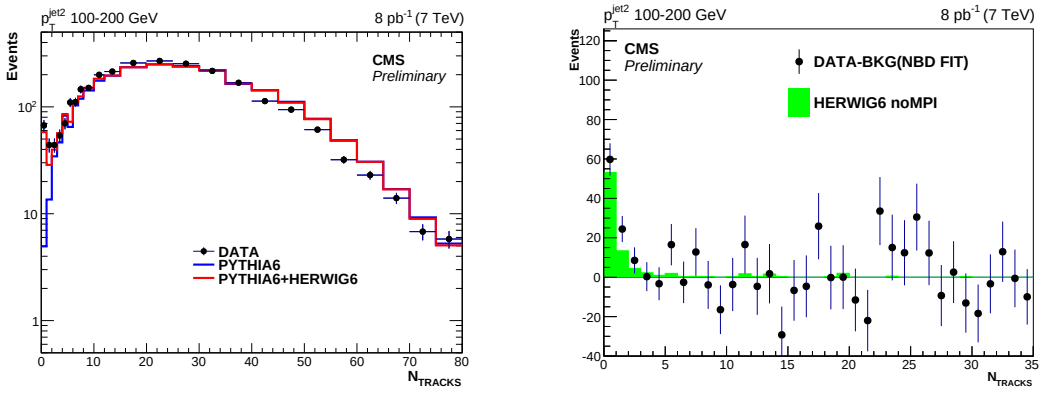

Figure 6: Left: charged multiplicity distribution for the highest p_T jet interval, compared to the HERWIG6 and PYTHIA6 predictions. Right: background-subtracted charged multiplicity distribution in the highest p_T interval, compared to the HERWIG6 predictions for events without an additional multiparton interaction.

The yield of jet-gap-jet events is shown in Fig. 7 left as a function of the transverse momentum of the second-leading jet and compared to earlier results by D0 [12] and CDF [13]. The decrease of the gap fraction with increasing center-of-mass energy is in agreement with the earlier observation by the TEVATRON experiments (when $\sqrt{s}$ increases from 0.63 GeV to 1.8 GeV). It can be explained by the enhancement with energy of rescattering processes, which destroy the rapidity gap. In Fig. 7 right the data are compared to the theoretical predictions of the Mueller and Tang (MT) model [2] , calculated with HERWIG for pure jet-gap-jet events (no simulation of MPI). The MT model does not describe the rise of the gap fraction with p_T, as already observed for the TEVATRON results. Moreover, it underestimates the CMS data.

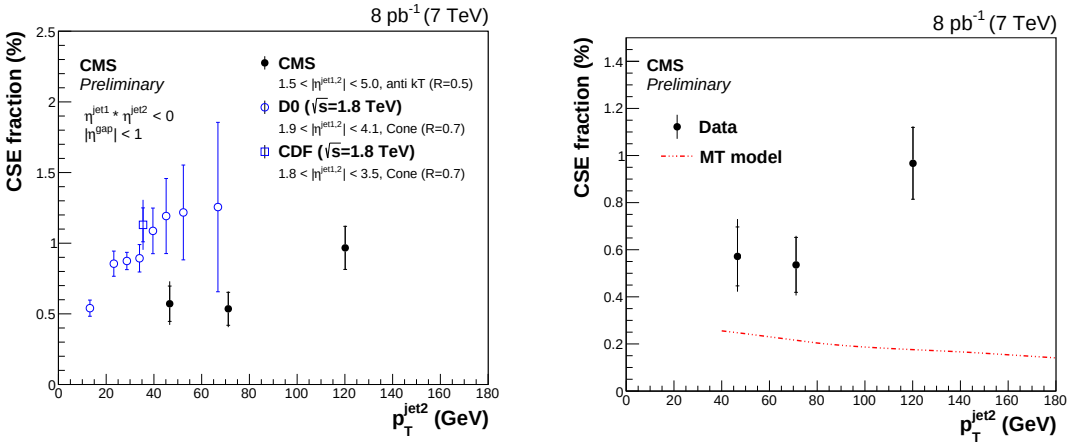

Figure 7: Left: yield of jet-gap-jet events as a function of the transverse momentum of the second-leading jet as measured by CMS at $\sqrt{s}$ of 7 TeV and by D0 [12] and CDF [13] at 1.8 TeV. Right: the CMS measurement compared to the predictions by the Mueller and Tang model [2].

References

[1] V. N. Gribov and L. N. Lipatov, Sov. J. Nucl. Phys. 15 (1972) 438; G. Altarelli and G. Parisi, Nucl. Phys. B126 (1977) 298; Y. L. Dokshitzer, Sov. Phys. JETP 46 (1977) 641.

[2] A. H. Mueller and W. -K. Tang, Phys. Lett. B284 (1992) 123.

[3] CMS Collaboration, JINST 3 (2008) S08004.

[4] CMS Collaboration, Phys. Rev. D 92 (2015) 012003.

[5] R. Ciesielski and K. Goulianos, arXiv:1205.1446.

[6] T. Sjostrand, S. Mrenna, and P.Z. Skands, Comput. Phys. Commun. 178 (2008) 852-867.

[7] ALICE Collaboration, Eur. Phys. J. C 73 (2013) 2456.

[8] ATLAS Collaboration, Eur. Phys. J. C 72 (2012) 1926.

[9] T. Sjostrand, S. Mrenna and P. Skands, JHEP **05** (2006) 026.

[10] G. Corcella et al., JHEP 0101 (2001) 010.

[11] J. Butterworth, J. R. Forshaw and M. Seymour, Z. Phys. C72 (1996) 637.

[12] D0 Collaboration, Phys. Lett. B440 (1998) 189.

[13] CDF Collaboration, Phys. Rev. Lett. 80 (1998) 1156.